MRI detection of glycogen *in vivo* by using chemical exchange saturation transfer imaging (glycoCEST)

Peter C. M. van Zijl*†‡, Craig K. Jones*†, Jimin Ren§, Craig R. Malloy§¶, and A. Dean Sherry‡§

*Division of Magnetic Resonance Research, Neurology Section, Russell H. Morgan Department of Radiology and Radiological Science, Johns Hopkins Medical Institutions, Baltimore, MD 21205; †F. M. Kirby Research Center for Functional Brain Imaging, Kennedy Krieger Institute, Baltimore, MD 21205; §Advanced Imaging Research Center, University of Texas Southwestern Medical Center, Dallas, TX 75390-8568; and ¶VA North Texas Health Care System, Dallas, TX 76216

Communicated by Robert G. Shulman, Yale University, New Haven, CT, January 12, 2007 (received for review September 18, 2006)

Detection of glycogen *in vivo* would have utility in the study of normal physiology and many disorders. Presently, the only magnetic resonance (MR) method available to study glycogen metabolism *in vivo* is ^{13}C MR spectroscopy, but this technology is not routinely available on standard clinical scanners. Here, we show that glycogen can be detected indirectly through the water signal by using selective radio frequency (RF) saturation of the hydroxyl protons in the 0.5- to 1.5-ppm frequency range downfield from water. The resulting saturated spins are rapidly transferred to water protons via chemical exchange, leading to partial saturation of the water signal, a process now known as chemical exchange saturation transfer. This effect is demonstrated in glycogen phantoms at magnetic field strengths of 4.7 and 9.4 T, showing improved detection at higher field in adherence with MR exchange theory. Difference images obtained during RF irradiation at 1.0 ppm upfield and downfield of the water signal showed that glycogen metabolism could be followed in isolated, perfused mouse livers at 4.7 T before and after administration of glucagon. Glycogen breakdown was confirmed by measuring effluent glucose and, in separate experiments, by ^{13}C NMR spectroscopy. This approach opens the way to image the distribution of tissue glycogen *in vivo* and to monitor its metabolism rapidly and noninvasively with MRI.

glucose | liver | water imaging | noninvasive

Glycogen, the primary storage form of glucose in mammalian tissues, plays a central role in systemic glucose homeostasis. Abnormalities of glycogen metabolism occur in certain rare inherited disorders (1), but glycogen content may also be abnormal in conditions such as obesity, insulin resistance, and type 2 diabetes (T2D). Thus, methods to quantify glycogen *in vivo* will be key to understanding the pathophysiology of these common diseases. Because there are numerous practical disadvantages to measuring glycogen by tissue biopsy in humans, there has been widespread interest in detection of glycogen *in vivo* by ^{13}C magnetic resonance (MR) spectroscopy (MRS) in multiple organs, including the heart (2), liver (3), skeletal muscle (4), and brain (5). Although glycogen is a large molecule, ^{13}C NMR allows accurate measurements of glycogen content in liver (6) and in skeletal muscle (7), presumably because internal motions remain sufficiently unrestricted *in vivo* (8). Detection of glycogen using ^{1}H NMR also has been demonstrated (9–11). With these MRS methods, a wide dynamic range of glycogen levels has been observed. For example, in the liver, the typical concentration in healthy humans shortly after a meal ranges from 318 mM (12) to 470 mM (13) glucosyl units and decreases to ≈200–300 mM after moderate fasting (14). In an early clinical application, Magnusson *et al.* (3) found that hepatic glycogen is much lower in T2D patients compared with controls after an overnight fast. Perhaps more importantly, ^{13}C MRS shows that hepatic glycogen is resynthesized more slowly after a meal among patients with insulin-dependent diabetes and fails to reach the same high levels found in normal controls (15). This finding suggests that diabetic patients have some kinetic limitation related to glycogen synthesis in liver. Interestingly, the opposite trend has been found among patients with T2D by using alternative methods in which hepatic glycogen content as estimated from a glycemic response to glucagon was elevated (16) and hepatic glycogen measured chemically in obese subjects was increased (17). These observations are consistent with two common animal models of diabetes in which glycogen was abnormally high in the *ob*/*ob* leptin-deficient mouse (18) as well as in the Zucker diabetic fatty rat (19). Paradoxically, hepatic glycogen increased even further during prolonged fasting (20) in these animals. It is difficult to reconcile these reports or to distinguish between increased hepatic gluconeogenesis versus excess hepatic glycogen stores and glycogenolysis using current measurement methods. Therefore, there is a strong need to develop alternative approaches that can image glycogen and monitor glycogen metabolism in humans.

Currently, the only noninvasive approach to determine the glycogen content of the *in vivo* liver is ^{13}C MRS. With this method, the concentration of glycogen is detected directly by the natural abundance ^{13}C C_1 of glycogen. However, ^{13}C MRS is available only in specialized research sites because it requires equipment not available on most instruments. Quantification of the glycogen content in liver and other organs would be useful for a wide variety of applications if it could be performed with a standard clinical MRI scanner.

We hypothesized that indirect detection of glycogen via the water resonance in MRI should be possible by exploiting chemical exchange between the hydroxyl protons and the water protons. To investigate this possibility, we used chemical exchange saturation transfer (CEST) (21–23) techniques in which selective radio frequency (RF) irradiation of solute protons is detected through progressive saturation of the water signal as a function of time. Because hydroxyl protons exchange rather quickly with solvent protons [exchange rate, $k > 10^3$ per s, (24)], saturated hydroxyl spins on glycogen transfer rapidly to the water protons and thereby reduce the intensity of the water signal. When irradiating for a period of a few seconds, a cumulative saturation of the water signal occurs. This simple sensitivity enhancement approach has previously been demonstrated for small molecules in phantoms (25), paramagnetic agents *in vitro* (25–27) and *ex vivo* (28), protein fragments *in vitro* (22, 29) and *in vivo* (30, 31), and nucleic acids *in vitro* (32). It is not obvious that CEST could be applied to detect

Author contributions: P.C.M.v.Z. and C.K.J. contributed equally to this work; P.C.M.v.Z., C.K.J., C.R.M., and A.D.S. designed research; P.C.M.v.Z., C.K.J., J.R., and A.D.S. performed research; P.C.M.v.Z., C.K.J., J.R., and A.D.S. analyzed data; and P.C.M.v.Z., C.R.M., and A.D.S. wrote the paper.

Conflict of interest statement: P.C.M.v.Z. and C.K.J. have filed a patent application for the glycoCEST technology.

Abbreviations: CEST, chemical exchange saturation transfer; glycoCEST, glycogen imaging with CEST; MT, magnetization transfer; MTR_{asym}, MT asymmetry ratio; MR, magnetic resonance; MRS, MR spectroscopy; RF, radio frequency.

‡To whom correspondence may be addressed. E-mail: pvanzijl@mri.jhu.edu or sherry@utdallas.edu.

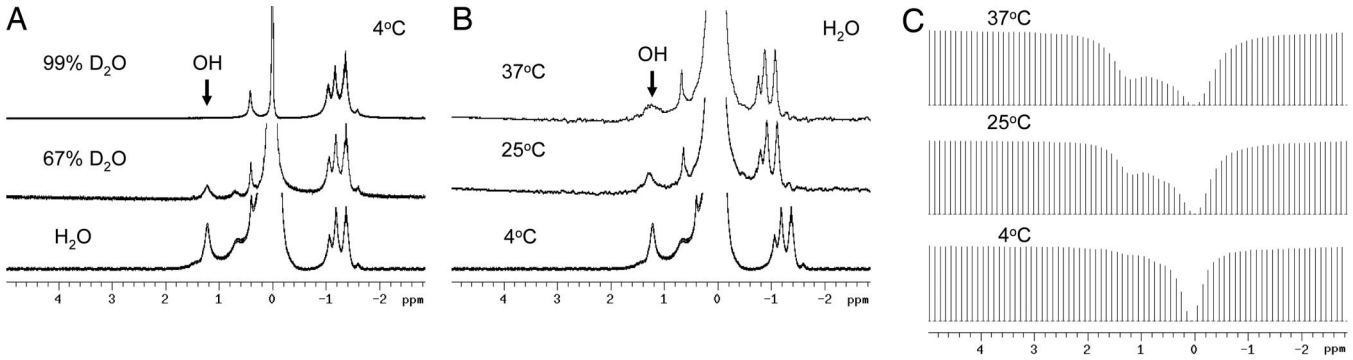

Fig. 1. Assignment of glycogen hydroxyl resonances and demonstration of increased sensitivity in CEST versus conventional MRS. (*A* and *B*) ^{1}H NMR spectra of 200 mM glycogen acquired at 9.4 T in unbuffered H_2O (pH = 7) as a function of ^2H_2O concentration at 4°C (*A*) and as a function of temperature (*B*). The water frequency was arbitrarily set to 0.0 ppm, as is common for CEST experiments. The OH resonances at 1.2 and 0.7 ppm (2:1 ratio) downfield from water disappear in ^2H_2O and broaden at higher temperature. (*C*) Interestingly, corresponding *Z* spectra show increased glycogen detectability at higher temperature.

hydroxyl groups because OH protons exchange quite rapidly and have only a small chemical shift difference with bulk water protons. Conventional NMR knowledge teaches that to be able to selectively irradiate a solute proton in the spectrum, it should be sufficiently separated in resonance frequency (chemical shift difference: $\Delta\omega = 2\pi\Delta\nu$, with ν in s^{-1} and ω in rad/s) from water protons to adhere to the so-called slow MR exchange condition, $\Delta\omega \gg k$. Because the glycogen hydroxyl protons resonate ≈0.5–1.5 ppm from water ($\Delta\omega \approx$ 630–1,890 rad/s at a field of 4.7 T), exchange is intermediate to fast on the MR time scale, and the hydroxyl protons are not visible in a standard proton spectrum under buffered physiological conditions (pH ≈7.1–7.3; temperature, ≈37°C). However, as demonstrated herein, sufficient saturation occurs within the brief lifetime that the hydroxyl protons remain on glycogen such that a cumulative effect is detected in the water signal when RF irradiation is applied to the hydroxyl protons. After assignment of the OH resonances, this is first demonstrated in phantoms at magnetic field strengths ranging from 4.7 to 9.4 T followed by implementation of glycogen imaging with CEST (glycoCEST) to monitor glycogen breakdown in the perfused mouse liver after administration of glucagon.

Results and Discussion

Phantom Studies. Fig. 1 shows high-resolution ^{1}H NMR spectra of glycogen in water as a function of added ^2H_2O (Fig. 1*A*) and temperature (Fig. 1*B*). At 4°C, a well defined resonance is visible at 1.2 ppm downfield from water, which disappears upon addition of ^2H_2O (Fig. 1*A*). In 67% ^2H_2O, another exchangeable proton is visible at 0.7 ppm, with approximately half the intensity of the 1.2-ppm peak. These signals are well separated from a single resonance at 0.4 ppm downfield of water, previously assigned to the nonexchangeable $-C_1H$ resonance of the α(1–4) glycosidic linkage (9). Based on their disappearance in ^2H_2O, their signal intensities, and basic chemical shift considerations, we assign these to the two OH ring protons (C2 and C3) and the CH_2OH sidegroup (C6) in glycogen. The linewidth of the −OH resonance at 1.2 ppm is reasonably sharp at 4°C and gradually broadens when the temperature is increased to 37°C, again characteristic of −OH protons in relatively slow exchange with free water protons.

In Fig. 1*C*, so-called *Z* spectra (33) of this same sample in H_2O are shown as a function of temperature. These spectra reflect the water intensity that remains when saturating with frequency-selective RF irradiation at different offsets with respect to the water resonance, which is arbitrarily set at 0 ppm. The *Z* spectrum at 4°C shows a minor dip at 1.2 ppm, which is due to CEST effect, again consistent with relatively slow proton exchange for the OH groups. Interestingly, although the temperature-based increase in −OH exchange rate reduces visibility in the proton NMR spectra (Fig. 1*B*), the detection sensitivity is enhanced in the *Z* spectra (Fig. 1*C*) because of the dependency of the CEST effect on the proton exchange rate. When using a glycogen solution in PBS buffer, the exchange rate increases dramatically and the −OH resonances are barely visible in the proton spectrum because of severe line broadening (data not shown). However, the −OH resonances are still very apparent in the *Z* spectra, as long as the RF irradiation hits this broadened resonance, which still is present under intermediate exchange conditions. Similar to conventional spectra, though, the detectability becomes better at higher magnetic fields. Interestingly, in the case of *Z* spectra, this field-dependent improvement is not particularly because of better adherence to the slow-exchange condition ($\Delta\omega \gg k$) but because the resonances close to water are separated more in frequency from the water line, reducing the overlap with regions of direct water saturation when keeping the bandwidth of the selective irradiation similar. This effect is illustrated in Fig. 2.

To demonstrate that the CEST effect changes with glycogen concentration, *Z* spectra were collected on samples ranging in concentration from 10 to 200 mM in PBS buffer (Fig. 3*A*). For comparison, equal concentrations of glucose were also studied (Fig. 3*B*). The data illustrate that glucose can also be detected by *Z* spectroscopy at 37°C with similar sensitivity but that glucose

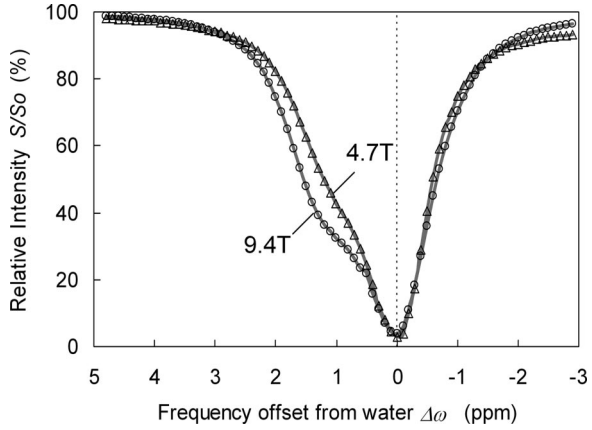

Fig. 2. *Z* spectra of 200 mM glycogen in PBS buffer at 37°C (pH 7.4) acquired at 9.4 T (5-mm NMR tube) and 4.7 T (spherical bulb) by using a 10-s presaturation pulse and with a B_1 of 1.9 μT and repetition time of 28 s. Notice the better definition of the CEST effect at a higher field due to the increased chemical shift difference in hertz.

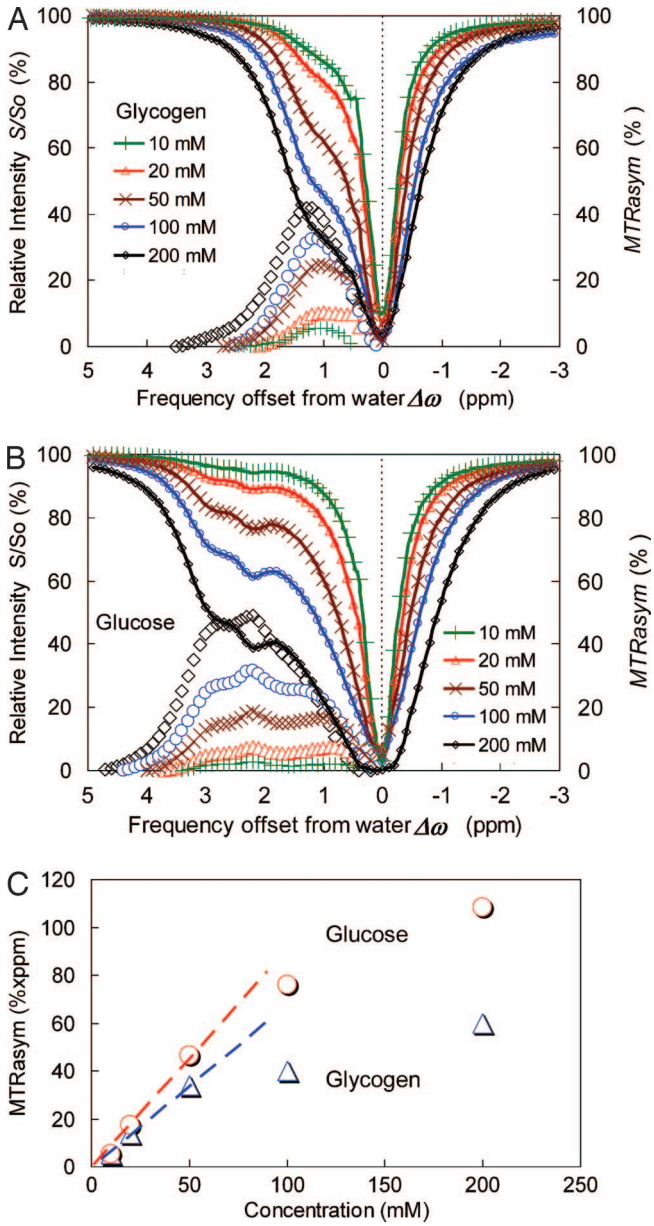

Fig. 3. Detection of glycogen and glucose in phantoms by using glycoCEST. (*A* and *B*) *Z* spectra and MTR_{asym} plots for samples of glycogen (*A*) and glucose (*B*) in PBS buffer at 37°C (pH 7.4). Notice the visibility of multiple OH resonances in the glucose sample. (*C*) When plotting the MTR_{asym} integral as a function of concentration, linear dependence is found at a lower concentration but not at higher values (see text).

has more exchangeable protons than glycogen and that the CEST effect is spread out over a larger range of frequencies. Interestingly, three different resonances for the −OH groups in glucose are apparent in the *Z* spectra, especially at higher concentration.

Although it is evident from both samples that the CEST effect becomes more pronounced at higher concentrations, it is difficult to quantify this effect because of the close proximity with regions affected by direct water saturation. The magnitude of this effect can therefore be better described quantitatively in terms of a magnetization transfer (MT) asymmetry ratio (MTR_{asym}) parameter, defined as

$$MTR_{asym}(\Delta\omega) = S(-\Delta\omega)/S_0 - S(\Delta\omega)/S_0, \quad [1]$$

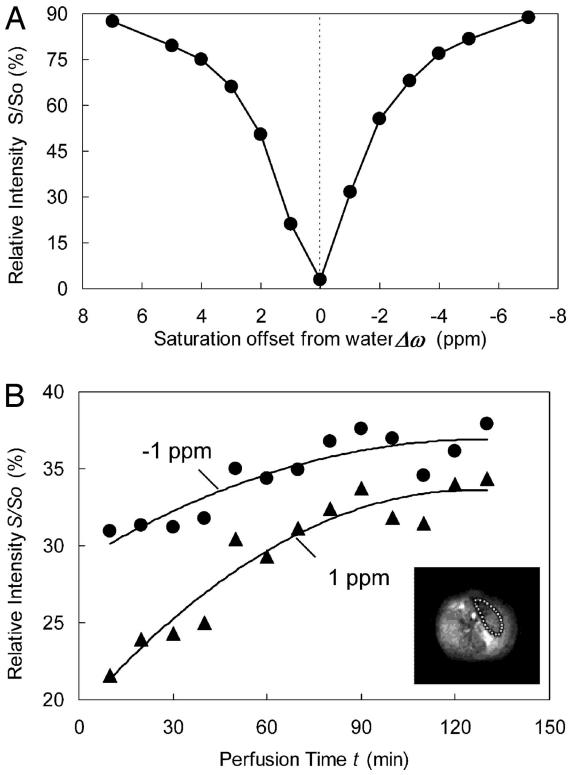

Fig. 4. *Z* spectra from a region of interest in a perfused liver at 4.7 T, acquired by using a 200-ms saturation pulse and a B_1 of 3 μT. When adding glucagon to the perfusate, the intensity of the saturated water signal at 1 ppm offset from water (circles) increases ≈150% more during the 130-min perfusion period than the saturated water signal at −1 ppm (triangles). The difference between these two intensities reflects depletion of glycogen.

where Δω is the difference between the irradiation frequency and the water frequency and $S(\Delta\omega)$ and S_0 are the water intensities after a long presaturation pulse at the offset frequency and at a very large offset at which water is not affected, respectively. In this approach, it is assumed that the direct water saturation is symmetric with respect to 0 ppm and that it can be subtracted out. These MTR_{asym} curves also are shown in Fig. 3 *A* and *B*, and the integrated areas under them are displayed in Fig. 3*C*. It is clear that this MTR_{asym} area is proportional to concentration but that the relationship is not strictly linear. One would not expect the magnitude of the CEST effect to be linear with concentration because, like any saturation phenomenon, the effect can only approach a maximum of 100%. Thus, for higher exchange rates, this maximum will be reached at lower concentrations, and the amount of saturation depends on the effect of both parameters. An exact quantitative description of the CEST effect is possible through use of the Bloch equations using a two-compartment model including exchange and RF saturation (29, 34, 35). Under the assumption of slow exchange on the NMR time scale and for OH single-proton exchange rates (k), the CEST effect can be described analytically by

$$MTR_{asym}(\Delta\omega) = \frac{k \cdot x_{gl} \cdot \alpha(k, x_{gl})}{R_{1w} + k \cdot x_{gl}} [1 - e^{-(R_{1w} + k \cdot x_{gl}) t_{sat}}], \quad [2]$$

in which $x_{gl} = n \cdot [gl]/(2[H_2O])$ is the fraction of exchangeable protons for glucose or glycogen, with $n = 5$ for glucose and ≤3 for glycogen, depending on the branching of the glycosyl links. The saturation factor $\alpha(k, x_{gl})$ is close to 1 at sufficiently high B_1 power but may reduce for rapidly exchanging protons because they cannot be saturated before exchanging. Water proton

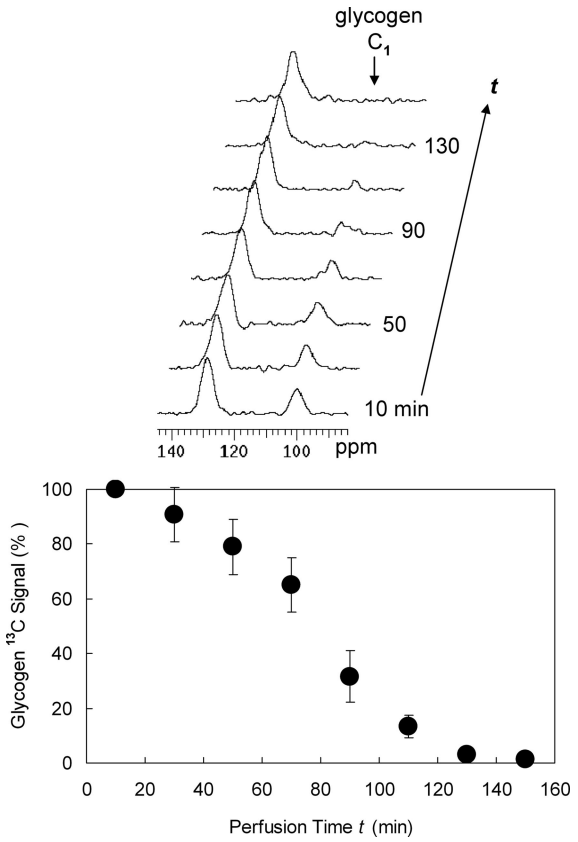

Fig. 5. ^{13}C NMR spectra of a liver from a fed mouse showing the disappearance of glycogen after glucagon administration. The resonance at 100 ppm is distinctive of C_1 of glycogen, whereas the resonance near 130 ppm is from unsaturated fats in liver (used here an internal standard only). The plot shows changes in intensity of the C_1 glycogen resonance after addition of glucagon ($n = 3$).

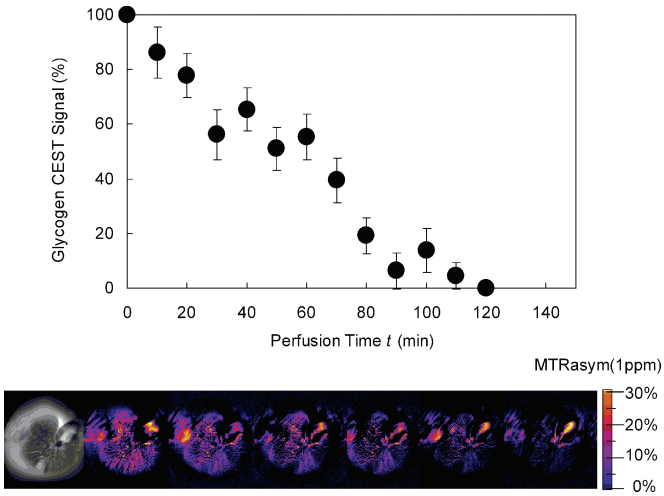

Fig. 6. glycoCEST imaging of a perfused fed-mouse liver at 4.7 T and 37°C. The first image (gray scale) marks the beginning of perfusion ($t = 0$) with glucose-free media containing 500 pg/ml glucagon. The liver tissue is darkened because of the CEST effect from presaturation at 1.0 ppm for 1 s at 3.0 μT. Upon further perfusion with glucagon, the liver signal increased, corresponding to a decrease in CEST effect. The colorized glycoCEST images as a function of time during perfusion show the relative CEST intensity [MTR_{asym} (1 ppm)] of liver tissue as a function of perfusion time. The color scale shows that there are regions of liver where the initial asymmetry difference between ± 1 ppm is as high as 55% (orange pixels) and as low as 5% (blue pixels). With time, as glycogen disappears, the CEST images become more uniformly dark blue, corresponding to minimal glycogen. The corresponding glycogen depletion for a homogeneous region of interest is quantified in the graph ($n = 4$).

longitudinal relaxation ($R_{1w} = 1/T_{1w}$) and back exchange of saturated water protons reduce the CEST effect, which occurs for fast exchange and high concentrations of exchangeable protons. Unfortunately, glycogen has a chemical shift difference with water that is smaller than the OH exchange rate, and it is not possible to use this simple analytical solution to fit the concentration data, not even at low concentrations. Exact fits can be obtained by numerically fitting the complete set of six Bloch equations (29), which is beyond the purpose of this paper. Another potential complication for glycogen quantification is the exchange of saturated protons between different OH groups on this molecule, similar to that found recently in other complexes with OH groups (36). Such an effect may reduce the glycoCEST effect and would have to be described by a three-compartment model.

It is of interest to note that, although the CEST spectra of glycogen and glucose at equivalent concentrations overlap, it would still be possible to study glycogen in many tissues. For instance, given that a typical intracellular concentration of glucose in liver is likely not >1–2 mM, whereas that of glycogen in liver from a fed animal is on the order of 176–390 μmol per gram of wet tissue (≈200–300 mM) (37), any MTR_{asym} measured at an offset of 1.2 ppm in liver tissue would have an insignificant contribution from free glucose compared with that from glycogen.

Liver Studies. To evaluate whether glycogen detection is feasible in tissue, we performed CEST experiments on perfused livers isolated from fed mice and monitored glycogen metabolism before and after addition of glucagon, the natural hormone used to stimulate glycogenolysis. Fig. 4*A* illustrates a typical *Z* spectrum of a region of interest in a mouse liver before the addition of glucagon. Notice that, similar to Figs. 2 and 3*A*, there is a difference in relative water intensity after presaturation pulses are applied at ± 1 ppm, reflecting a contribution from glycogen saturation transfer to the water signal at +1 ppm. The plots in Fig. 4*B* show the intensities of the offset frequencies (± 1 ppm) as a function of time after glucagon administration. Interestingly, although there was an increase in water intensity at both offsets, the increase was much larger at +1 ppm, which we attribute to glycogenolysis stimulated by glucagon. The small increase at the reference frequency is tentatively attributed to a small increase in water content during ischemia, lengthening T_2 and thus reducing the direct saturation effect. These results suggest that glycogen is largely depleted after ≈120 min under these experimental conditions. The observation that intensity of the water signal at ± 1 ppm remains unequal even after depletion of glycogen may be due to several causes. First of all, although the water resonance was centered at the start of the experiment, field differences (inhomogeneities) between perfusate and liver or between areas of different magnetic susceptibility within the liver may cause the centering of the *Z* spectrum to be imperfect. Second, tissues have a baseline conventional MT effect that may also be asymmetric with respect to the water resonance (e.g., a few percent MTR_{asym} has been reported in brain (30, 38). Third, additional CEST contributions by other undefined exchange molecules in tissue that are unaffected by glucagons may contribute in principle. Because the remaining asymmetry is only a few percent, i.e., similar to previous tissue studies, we ascribe the phenomenon mainly to the second effect.

To verify that the changes described above arise from liver glycogen, two further experiments were performed. Because the perfusate in the experiments described above was initially free of glucose, verification that glycogen was being broken down in

response to glucagon was done by analyzing the perfusate for glucose over this same time period. Those analyses showed that glucose in the perfusate spiked shortly after glucagon administration and then gradually decreased over the 120-min perfusion period. The glucose concentration in the total volume of perfusate accumulated during the 120-min perfusion period (120 min × 8 ml/min = 960 ml) was ≈0.15 mM, corresponding to ≈144 μmol (0.15 mM × 960 ml) of glucose released from each liver on average. In separate experiments, livers from fed mice were perfused under conditions identical to those described above and freeze-clamped after exposure to glucagon for 120 min. Glycogen isolated from those frozen tissues averaged 37 ± 22 μmol per gram of wet tissue. In comparison, freshly isolated liver tissue contained 180 ± 8 μmol of glycogen per gram of wet tissue, so the difference quantitatively agrees with the amount of glucose found in the perfusate. Thus, the difference in water intensities after presaturation pulses at ±1 ppm can be ascribed to glucagon-induced glycogenolysis.

To validate this conclusion, we also measured glycogen in mouse livers by using ^{13}C NMR, the gold standard for glycogen in tissue. The stacked plot of Fig. 5 shows the nicely resolved natural abundance C_1 resonance of glycogen (100 ppm) before and after glucagon administration. Given that liver glycogen is known to be 100% visible by ^{13}C NMR (6, 8), these data demonstrate that glycogen indeed disappears after exposure to glucagon and is essentially below the detection limits of ^{13}C NMR after ≈120 min. This result is in agreement with the changes in CEST described above.

Given this important validation, we then turned to developing a protocol for glycoCEST. Fig. 6 illustrates glycoCEST images of a perfused mouse liver during glucagon-initiated breakdown of glycogen. The glycoCEST images were generated as follows. First, a series of spin-echo images were collected from a single 3-mm slice of liver after a 1-s presaturation pulse (B_1 = 3 μT) applied at +1 ppm. Each image required 8.5 min. The intensity of the liver tissue was darker in images collected with a presaturation pulse turned on, compared with the image intensities in images without presaturation. The difference in these intensities [MTR_{asym} (1 ppm)] decreased over a period of ≈120 min and remained constant thereafter. These final images must therefore represent the water intensity of a glycogen-depleted liver. These MTR_{asym} (1 ppm) changes with time referenced to the final time point are presented as colorized glycoCEST images in Fig. 6. The accompanying plot shows average values for these time-dependent changes in image intensity (region of interest confined to liver tissue only) for four livers. These glycoCEST images are interesting in that they not only illustrate depletion of glycogen with time, but the intensity variations within any individual glycoCEST image suggest that glycogen may not be uniformly distributed in all regions of liver (39). Of course it has to be kept in mind that field inhomogeneities may shift frequencies around, thereby leading to some potential artifactual signal spikes in CEST images. Intensity spikes that change as a function of time during perfusion are visible in the liver, which we attribute to field inhomogeneity variation due to motion from slightly uneven perfusate effluent. Corrections for such effects can be implemented, e.g., when acquiring a reference field map or voxel-by-voxel Z spectra.

In summary, we have demonstrated that liver glycogen can be detected by using CEST methods after partial saturation of the large number of −OH groups on the polymer. This result was unexpected because proton exchange between the glycogen −OH protons and bulk water was anticipated to be too fast compared with the very small chemical shift difference between these two species. Nevertheless, the data presented here show conclusively that glycogen can be imaged by using CEST principles. The magnitude of the glycoCEST effect may depend on factors other than glycogen concentration that influence the CEST efficiency, including glycogen size and molecular architecture and contribution from asymmetry in the conventional MT effect. Nevertheless, this technique is important because it offers the possibility of monitoring glycogen metabolism in tissue with MRI.

Materials and Methods

Perfused Liver Studies. Studies were approved by the Institutional Animal Care and Use Committee at the University of Texas Southwestern Medical Center. C57BL6 female mice weighing 22 ± 2 grams (n = 7), either fasted (24 h with water access) or provided continuous access to standard laboratory chow, were anesthetized by i.m. injection of ketamine (Ketaset; Aveco, Fort Dodge, IA) before a mid-line laparotomy to expose the liver and portal circulatory system. The portal vein was cannulated and immediately perfused with physiological buffer containing heparin by using a peristaltic pump with a flow rate of 8 ml/min at 37°C. The nonrecirculating perfusate was a modified Krebs–Henseleit (KH) bicarbonate buffer (95% O_2/5% CO_2) consisting of 118 mM NaCl, 5 mM KCl, 1.2 mM $MgSO_4$, 25 mM $NaHCO_3$, 1.2 mM $CaCl_2$, and 0.2 mM octanoate (oxidative fuel source) but no glucose (unless otherwise specified). The hepatic vein and inferior vena cava were dissected, and the liver was carefully removed and suspended in a container positioned directly above a 2.5-cm ^{1}H surface coil. The average liver weight was 1.2 ± 0.1 g (n = 7). All livers were perfused with KH buffer containing 10 mM glucose during the isolation procedure and during coil tuning/matching and shimming. Perfusate was then switched to fresh KH buffer without glucose but with 500 pg/ml glucagon so that effluent perfusate could be collected and analyzed for glucose coming from the liver. The glucagon solution contained 0.1% BSA to stabilize the hormone from enzymatic degradation. Glucose in effluent perfusate was measured enzymatically by using glucose oxidase; perfusate oxygen and pH were measured by using a pH/blood gas analyzer (Instrumentation Laboratory, Lexington, MA). The average perfusate pH was 7.4 ± 0.1 (n = 7).

In separate experiments, livers from two mice were perfused on the bench at 37°C, one for 2 h with a modified glucose-free KH media containing 500 pg/ml glucagon and 0.2 mM octonoate and another for 5 min in the same modified glucose-free KH media but without glucagon. Livers were freeze-clamped (liquid N_2), pulverized with a mortar and pestle, extracted with 30% KOH, and precipitated with ethanol as described elsewhere (29). Isolated glycogen was hydrolyzed to glucose by using amyloglucosidase (Sigma–Aldrich, St. Louis, MO), and the resulting solution was assayed for glucose as described above.

Phantoms. Bovine liver glycogen (Type 1X″ G0885, CAS no. 9005-79-2; Sigma, St. Louis, MO) with an average molecular mass of 50 kDa was dissolved in water or in PBS (152 mM Na^+/9.6 mM P_i/pH 7.4). The concentration of glycogen is expressed in millimolar glucosyl units, with each glucosyl unit contributing 168 g/mol. For example, for a 100 mM solution of glycogen, 33.6 mg of glycogen was dissolved in 2 ml of PBS [33.6 mg/(168 mg/mmol × 2 ml) = 0.1 M).

MRI Acquisition. Proton-decoupled ^{13}C MRS was performed on perfused mouse livers in a 20-mm NMR tube on a 9.4-T vertical bore scanner (Inova; Varian, Palo Alto, CA). Proton-decoupled ^{13}C spectra were signal-averaged over a period of 20 min (^{13}C flip-angle, 50°; repetition time, 0.5 s). Z spectra were collected in a 5-mm NMR tube by using a high-resolution probe over a ±10-ppm range in steps of 0.1 ppm with a 10-s presaturation pulse (B_1 = 1.9 μT) followed by a 2-ms Z gradient pulse for dephasing residual transverse magnetization, and a 90° readout pulse. Repetition time was 28 s. All samples were maintained at 37°C. For the phantom at 4.7 T, a spherical bulb inside a transmit–receive Litz coil was measured with the same saturation power and duration.

CEST imaging of glycogen in isolated perfused mouse livers was performed by using a 4.7-T, 40-m bore Inova MRS/MRI animal system (Varian). A 2.5-cm surface coil placed under the perfusion chamber was used for excitation and reception. The imaging pulse sequence consisted of a Gaussian-shaped presaturation pulse (0.2 or 1 s, $B_1 = 3$ μT) followed by standard spin-echo imaging. Other parameters included the following: single slice 3 mm thick; repetition time, 2 s; time to echo, 13 ms; field of view, 30 mm; 64 $\times$ 64 matrix. CEST images were collected at $\pm$1.0 ppm from water.

Data Analysis. ^{13}C NMR spectra were phased, and the integral of the peak at 100 ppm (C_1 of glycogen) was compared between livers before and after the addition of glucagon. For the perfused liver studies, image processing was performed with ImageJ (http://rsb.info.nih.gov/ij). The mean and standard deviation of signal intensities in the MTR_{asym} (between $\pm$1 ppm irradiation) plots expressed in percent were calculated within a region of interest in the tissue. The glycoCEST effect was obtained by subtracting the MTR_{asym} image acquired at a given perfusion time point (t) from the reference image acquired at the end of perfusion ($t > 120$ min), when hepatic glycogen was assumed to be fully depleted.

We thank Mike McMahon, Assaf Gilad, Matthew Merritt, Chuck Storey, and Angela Milde for excellent technical assistance during various aspects of this study. This work was supported by National Institutes of Health Grants P41-RR02584, U24-DK16194, and HL-34557 and by Philips Medical Systems.

1. Wolfsdorf JI, Weinstein DA (2003) *Rev Endocr Metab Disord* 4:95–102.
2. Bottomley PA, Hardy CJ, Roemer PB, Mueller OM (1989) *Magn Reson Med* 12:348–363.
3. Magnusson I, Rothman DL, Katz LD, Shulman RG, Shulman GI (1992) *J Clin Invest* 90:1323–1327.
4. Cline GW, Petersen KF, Krssak M, Shen J, Hundal RS, Trajanoski Z, Inzucchi S, Dresner A, Rothman DL, Shulman GI (1999) *N Engl J Med* 341:240–246.
5. Oz G, Henry PG, Seaquist ER, Gruetter R (2003) *Neurochem Int* 43:323–329.
6. Gruetter R, Magnusson I, Rothman DL, Avison MJ, Shulman RG, Shulman GI (1994) *Magn Reson Med* 31:583–588.
7. Taylor R, Price TB, Rothman DL, Shulman RG, Shulman GI (1992) *Magn Reson Med* 27:13–20.
8. Zang LH, Laughlin MR, Rothman DL, Shulman RG (1990) *Biochemistry* 29:6815–6820.
9. Zang LH, Rothman DL, Shulman RG (1990) *Proc Natl Acad Sci USA* 87:1678–1680.
10. Chen W, Avison MJ, Zhu XH, Shulman RG (1993) *Biochemistry* 32:11483–11487.
11. Chen W, Zhu XH, Avison MJ, Shulman RG (1993) *Biochemistry* 32:9417–9422.
12. Taylor R, Magnusson I, Rothman DL, Cline GW, Caumo A, Cobelli C, Shulman GI (1996) *J Clin Invest* 97:126–132.
13. Petersen KF, Price T, Cline GW, Rothman DL, Shulman GI (1996) *Am J Physiol* 270:E186–E191.
14. Petersen KF, Cline GW, Gerard DP, Magnusson I, Rothman DL, Shulman GI (2001) *Metabolism* 50:598–601.
15. Hwang JH, Perseghin G, Rothman DL, Cline GW, Magnusson I, Petersen KF, Shulman GI (1995) *J Clin Invest* 95:783–787.
16. Clore JN, Post EP, Bailey DJ, Nestler JE, Blackard WG (1992) *J Clin Endocrinol Metab* 74:660–666.
17. Muller C, Assimacopoulos-Jeannet F, Mosimann F, Schneiter P, Riou JP, Pachiaudi C, Felber JP, Jequier E, Jeanrenaud B, Tappy L (1997) *Diabetologia* 40:463–468.
18. Turner SM, Linfoot PA, Neese RA, Hellerstein MK (2005) *Acta Diabetol* 42:187–193.
19. Jin ES, Burgess SC, Merritt ME, Sherry AD, Malloy CR (2005) *Am J Physiol* 288:E654–E662.
20. Triscari J, Bryce GF, Sullivan AC (1980) *Metabolism* 29:377–385.
21. Ward K, Balaban RS (2000) *Magn Reson Med* 44:799–802.
22. Goffeney N, Bulte JW, Duyn J, Bryant LH, Jr, van Zijl PC (2001) *J Am Chem Soc* 123:8628–8629.
23. Zhou J, van Zijl PCM (2006) *Progr NMR Spectr* 48:109–136.
24. Liepinsh E, Otting G (1996) *Magn Reson Med* 35:30–42.
25. Zhang S, Winter P, Wu K, Sherry AD (2001) *J Am Chem Soc* 123:1517–1518.
26. Aime S, Barge A, Delli Castelli D, Fedeli F, Mortillaro A, Nielsen FU, Terreno E (2002) *Magn Reson Med* 47:639–648.
27. Aime S, Delli Castelli D, Fedeli F, Terreno E (2002) *J Am Chem Soc* 124:9364–9365.
28. Aime S, Carrera C, Delli Castelli D, Geninatti Crich S, Terreno E (2005) *Angew Chem Int Ed Engl* 44:1813–1815.
29. McMahon MT, Gilad AA, Zhou J, Sun PZ, Bulte JW, van Zijl PC (2006) *Magn Reson Med* 55:836–847.
30. Zhou J, Payen J-F, Wilson DA, Traystman RJ, van Zijl PC (2003) *Nat Med* 9:1085–1090.
31. Zhou J, Lal B, Wilson DA, Laterra J, van Zijl PC (2003) *Magn Reson Med* 50:1120–1126.
32. Snoussi K, Bulte JW, Gueron M, van Zijl PC (2003) *Magn Reson Med* 49:998–1005.
33. Hinton DP, Bryant RG (1996) *Magn Reson Med* 35:497–505.
34. Zhou J, Wilson DA, Sun PZ, Klaus JA, van Zijl PCM (2004) *Magn Reson Med* 51:945–952.
35. Woessner DE, Zhang S, Merritt ME, Sherry AD (2005) *Magn Reson Med* 53:790–799.
36. Woods M, Woessner DE, Zhao P, Pasha A, Yang MY, Huang CH, Vasalitiy O, Morrow JR, Sherry AD (2006) *J Am Chem Soc* 128:10155–10162.
37. Williamson DH, Brosnan J (1971) in *Methods in Enzymatic Analysis*, ed Bergmeyer HU (Chemie, Weinheim, Germany), Vol 4, pp 2266–2268.
38. Pekar J, Jezzard P, Roberts DA, Leigh JS, Jr, Frank JA, McLaughlin AC (1996) *Magn Reson Med* 35:70–79.
39. Jungermann K (1992) *Diabete Metab* 18:81–86.